Scripta Materialia 229 (2023) 115370

Contents lists available at ScienceDirect

Scripta Materialia

journal homepage: www.journals.elsevier.com/scripta-materialia

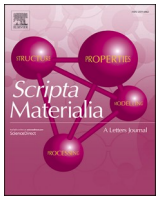

Atom probe analysis of $BaTiO_3$ enabled by metallic shielding

Se-Ho Kim [a,b,1,*], Kihyun Shin [c,d,e,1], Xuyang Zhou [a], Chanwon Jung [a], Hyun You Kim [d], Stella Pedrazzini [f], Michele Conroy [f], Graeme Henkelman [c], Baptiste Gault [a,f,*]

[a] Max-Planck-Institut für Eisenforschung, Max-Planck-Straße 1, 40237 Düsseldorf, Germany
[b] Department of Materials Science and Engineering, Korea University, Seoul 02841, Republic of Korea
[c] Department of Chemistry and the Oden Institute of Computational Engineering and Sciences, The University of Texas at Austin, Austin, TX 78712, United States
[d] Department of Materials Science and Engineering, Chungnam National University, Daejeon 34134, Republic of Korea
[e] Department of Materials Science and Engineering, Hanbat National University, Daejeon, 34158, Republic of Korea
[f] Department of Materials, Royal School of Mines, Imperial College London, SW7 2AZ London, UK

A B S T R A C T

Atom probe tomography has been raising in prominence as a microscopy and microanalysis technique to gain sub-nanoscale information from technologically-relevant materials. However, the analysis of some functional ceramics, particularly perovskites, has remained challenging with extremely low yield and success rate. This seems particularly problematic for materials with high piezoelectric activity, which may be difficult to express at the low temperatures necessary for satisfactory atom probe analysis. Here, we demonstrate the analysis of commercial $BaTiO_3$ particles embedded in a metallic matrix. Density-functional theory shows that a metallic coating prevents charge penetration of the electrostatic field, and thereby suppresses the associated volume change linked to the piezoelectric effect.

Since the discovery of the first ferroelectric material in the 1950s, $BaTiO_3$ [1] has been widely used across a range of applications for its piezoelectric properties [2] and in stacked ceramic capacitors, due to its high dielectric constant and low dielectric loss. For instance, the development of multilayer ceramic chip capacitors (MLCC) has improved volumetric efficiency, cost reduction, and performance such that their sales figures are the highest among fine-ceramic products.

Typically to fabricate a conventional MLCC, uniform-sized $BaTiO_3$ powders are cast on a conductive foil (*e.g.* Ni or Cu) and sintered. The key challenges to acquire reliable MLCCs from such a manufacturing process are having a constant dielectric layer thickness (several μm level in thickness) and the most careful control over the presence of impurities and/or dopants. Nowadays, the thickness of the capacitor cell can go down to a micron with high yield. However, the latter challenge is still a critical issue. The intrinsic properties of $BaTiO_3$ are easily modified by chemical doping. For example, less than 1 at.% of elemental modifier in the system may alter the Curie temperature and dielectric constant [3–6]. Extensive work has been reported on enhancing dielectric and ferroelectric properties of $BaTiO_3$ through Ba-site substitution using alkaline-earth [7–9] (Mg^{2+}, Ca^{2+}, Sr^{2+}) and rare-earth elements [10–12] (La^{3+}, Ce^{3+}, Dy^{3+}).

While there have been advances in analyzing constituent elements via inductively coupled plasma-optical emission spectrometry [13] and mass spectrometry [14], electron energy loss spectroscopy [15–17] and energy-dispersive X-ray spectroscopy (EDS) [18,19], time-of-flight secondary ion mass spectrometry [20], nuclear magnetic resonance spectroscopy [21], the direct, quantitative 3D elemental mapping of $BaTiO_3$ materials remains challenging. Atom probe tomography (APT) is expected to exhibit the required spatial resolution and elemental detection sensitivity. The physical principle on which the technique is based on field evaporation: an intense standing electric field (10^{10} V·m^{-1}) facilitates the removal and ionization of surface atoms from a needle-shaped specimens; the resulting ions are then accelerated by electrostatic forces toward a position-sensitive detector that measures their time-of-flight and impact coordinates, which are used for calculating a mass spectrum and reconstructing a 3D atom map, respectively [22].

Despite its potential to understand microstructural and chemical properties in perovskites, there have been only very few reports of APT analyses. In our preliminary work on a bulk $BaTiO_3$ perovskite material, five specimens were tested but all of them failed to acquire meaningful data (see Fig. S1). Inspired by the use of a metallic coating technique to prevent early specimen fracture or delithiation [23–25], here we propose a possible approach to facilitate APT measurement of piezoelectric $BaTiO_3$.

$BaTiO_3$ commercial powder (>99%, Sigma Aldrich) was sourced, with a specification sheet indicating un-specified impurity content of

* Corresponding authors.
E-mail addresses: s.kim@mpie.de (S.-H. Kim), b.gault@mpie.de (B. Gault).
[1] Contributed equally on this work

https://doi.org/10.1016/j.scriptamat.2023.115370
Received 8 December 2022; Received in revised form 6 February 2023; Accepted 13 February 2023
Available online 17 February 2023

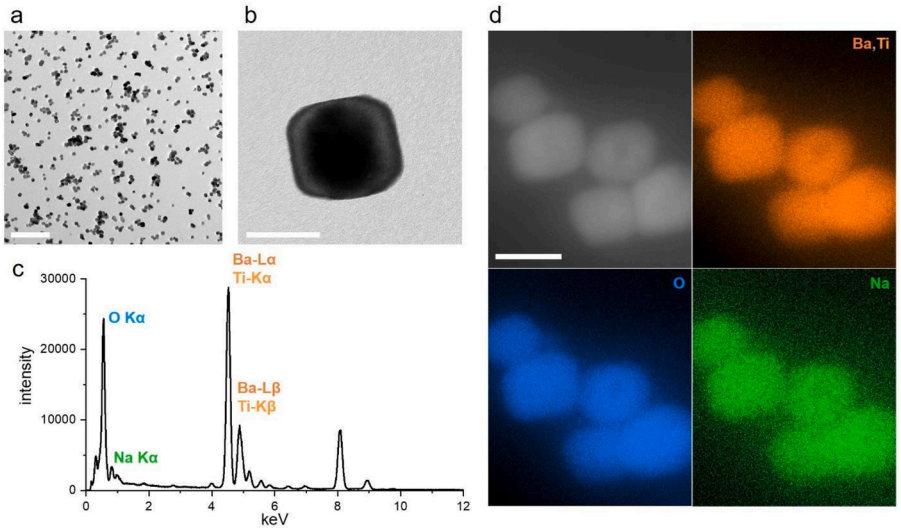

Fig. 1. Bright field TEM images of $BaTiO_3$ nanoparticles at (a) high and (b) low magnification. (c) Acquired EDS spectrum from the particle. A significant peak intensity at 8 keV corresponds to Cu from the commerical TEM grid. (d) Maps of TEM with EDS chemical composition on the particles: Ba and Ti (orange), O (blue), and Na (green). The scale bars are (a) 500 and (b-d) 30 nm. (For interpretation of the references to colour in this figure legend, the reader is referred to the web version of this article.).

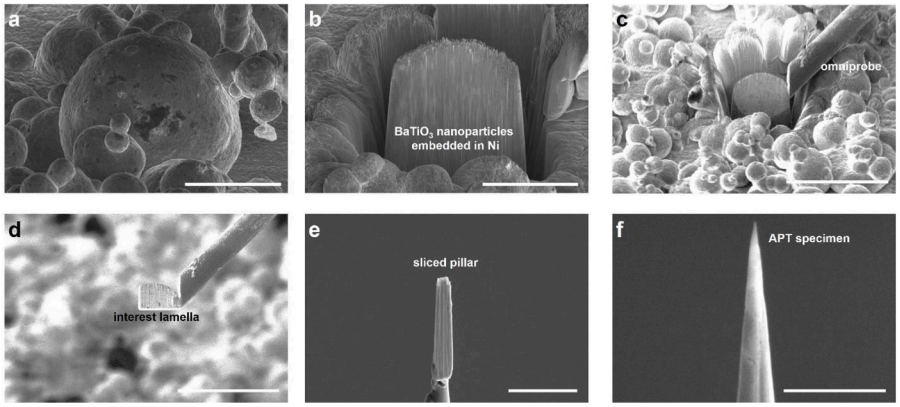

Fig. 2. APT specimen preparation for the Ni-coated $BaTiO_3$ powder sample: (a) 52° tilted SEM image of a selected protrusion region. (b) Trenches were milled 15 μm in depths on the front/back and the left-side of the region of interest with a width of 1 μm. (c) An L-shape horizontal cut was made at the bottom and side of the sample in 52° relative to the ion-beam column, after welding on an omni-probe. (d) The sectioned lamella was lifted-out. (e) Subsequently, the sample was welded with a FIB-Pt deposition on a commercial Si micro-post on only one side where a free cut was done. (f) Thereafter, a free-cut sample was annular milled from the top in decreasing diameters until the apex radius was below 100 nm and the capped Ni layer was removed. The white scale bars are (a,b) 20, (c,d) 50, (e) 10, (f) 1 μm.

10,000 ppm. Particles were first dispersed onto a Cu grid and imaged with a JEM-2200FS transmission electron microscopy (TEM; JEOL) operating at 300 kV equipped with an energy-dispersive X-ray analysis (EDS) system. Fig. 1a and 1b show bright-field TEM images of the commercial $BaTiO_3$ particles. The particles are 30 nm in size and have a chamfered cuboidal shape. The morphology of the particles is uniform, which is important to facilitate sintering, as the compactness decreases with a broader particle size/shape distribution [26]. EDS analysis was performed (Fig. 1c) with the characteristic X-ray peaks of the acquired spectrum were interpreted according to Ref [27]. The characteristic X-ray peaks of the main constituents (Ba, Ti) overlap substantially, making distinction challenging. Yet, despite a high background, signals from Na and Sr are detected (Fig. S2). Both elements are well reported to substitute Ba cation (A site in ABO_3 perovskite structure) [28,29]. Elemental mapping in Fig. 1d show a homogenous distribution of all elements. Nevertheless, as (S)TEM is a through-thickness projection microscopy, precise localization of each element is not readily possible without deploying highly advanced, electron tomography techniques.

To facilitate APT specimen preparation, we followed the protocol described by [30] to embed the powder, Fig. 2a, in a Ni-metallic matrix using a commercial nanoparticle depositor (Oxford Atomic. Ltd.), with a current of −19 mA. Ni is selected for the coating material simply because, in the MLCC manufacturing process, Ni is not only used as a capacitor electrode but also for encapsulating materials for sintered $BaTiO_3$ layers [31].

The pore-free composite was obtained after co-electroplating, suitable to prepare atom probe specimens, as shown in Fig. 2b. APT specimens were prepared using a FEI Quanta 3D dual-beam scanning-electron microscope/focused-ion beam (SEM/FIB) and following the *in situ* lift-out protocol outlined in ref [32]. and detailed in Fig. 2c–f. The atom probe data were acquired on a CAMECA LEAP 5000HR at a laser pulse frequency of 125 kHz, a base temperature of 60 K, a laser pulse energy of 80 pJ, and a detection rate of 0.5%.

Fig. 3a shows the 3D atom map of the $BaTiO_3$ particles embedded within the electroplated Ni matrix. The particle size was similar to the TEM observation. Fig. 3b displays the elemental distribution for an individual $BaTiO_3$ particle. Ca and Sr are detected as well as unexpected elements such as Na and Sc. Eiser and Beck had previously reported contamination by Sr and Ca in a similar material [33]. 1st order nearest-neighbor analysis of the major impurities, in Fig. 3c, show that they are randomly distributed, except for Na. A cylindrical region-of-interest was positioned normal to the particle's interface with the metallic matrix. The corresponding composition profile plotted in Fig. 3d indicates neither chemical partitioning nor segregation of the major elements, but Na shows an enrichment on the particle's surface.

To rationalize why the analysis of individual particles of $BaTiO_3$ embedded in Ni is successful, we performed GGA-level spin-polarized density-functional theory calculations with the Vienna ab initio simulation package (VASP) using a plane wave basis set with cut-off energy of 400 eV. The hybrid functional HSE06 was used to describe the electronic structure accurately [34] (see the SI for computational details).

Fig. 4a shows the charge density difference in the bare $BaTiO_3$ between with and without an applied electric field. The 2D mapping color codes the electron transfer processes, with electron-rich (in red) and

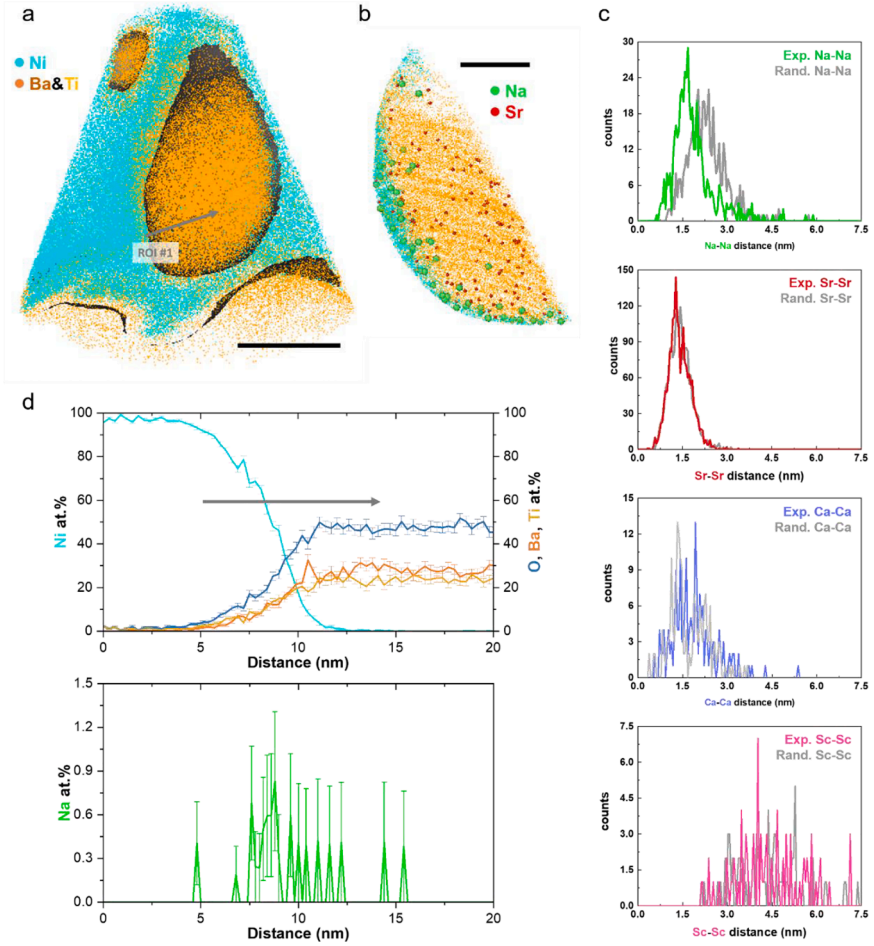

Fig. 3. (a) 3D atom map of $BaTiO_3$ particles embedded in Ni. (b) Distribution of constituent elements (Ba, Ti, Na, Sr) extracted from the atom map. (a,b) scale bars are 20 nm. (c) Nearest-neighbor displacement analyses of Na, Sr, Ca, and Sc elements. (d) 1D compositional analysis along the particle surface. A gray arrow marks the interest profile.

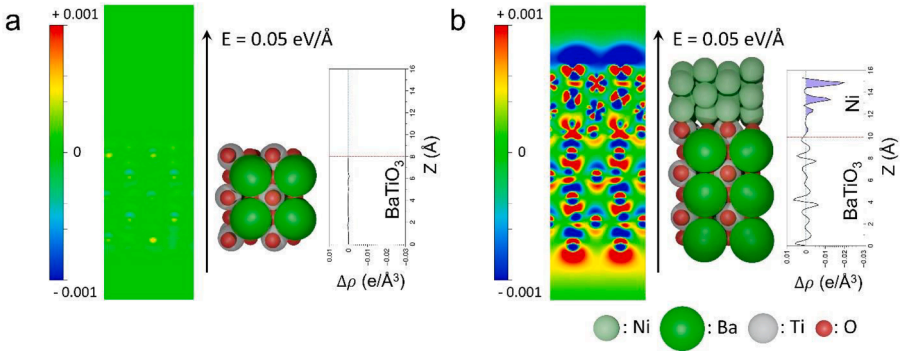

Fig. 4. Charge distributions under an applied electric field along the z-direction for (a) bare $BaTiO_3$ and (b) Ni-coated $BaTiO_3$. Each figure includes the charge-density change distribution before/after the applied field mapped in 2D with color mapping (left), illustrated structure model in identical atomic positions (center), and an electronic density changes along the z-direction (right).

electron-poor (in blue), with the corresponding atomic positions displayed on the side. The linear profile of the charge density change quantifies a very subtle change under an electric field of 0.05 eV/Å, with no localization of charges and a polarized material. The spontaneous polarization of $BaTiO_3$ along the direction of the applied electric field leads to lattice distortions, with a Ti off-centered displacement along the c-axis from the tetragonal structure with a rate of 149 pm V^{-1} [35]. With the conductive Ni layer on the $BaTiO_3$, shown in Fig. 4b, charges flow from the $BaTiO_3$ layers into the Ni, reverting the polarizations and shielding the external field. These calculations indicate that the conductive coating prevent field penetration as expected.

Typical field evaporation occurs at an electrostatic potential of a few kV, and under fields in the range of tens of V·nm^{-1} that cause strong electrostatic Maxwell stresses, making APT studies of brittle and non-conductive materials intrinsically challenging [36–39]. Additionally, most perovskite materials exhibit intrinsic piezoelectricity that is an electromechanical interaction between mechanical and electrical states; a polarization from external electric field generates an internal

mechanical load to the material. The combination of these factors, at the low temperature at which APT analyses are typically performed (25–80 K) facilitate early, brittle fracture of the specimen [40,41]. Heavily doped perovskites were successfully measured with APT, which could be attributed to the modified electronic structure [42], yet low yields had been reported [43]. The metallic coating suppressed the expression of the intrinsic piezoelectricity of $BaTiO_3$, which we believe explains the successful application of APT. Besides Ni, Co can be selected as a charge-shielding material for possible other candidate, as it is a mono-isotopic element and has a higher evaporation field than Ni [44]. The use of experimental conditions during APT analysis that would minimize the electrostatic field could facilitate successful data acquisition, *i.e.* a higher temperature raises from the pulsed laser illumination that could arise from the use of a shorter wavelength for instance.

A locally exposed surface of $BaTiO_3$ may experience piezoelectricity, however only from the one exposed surface, and not from all around a complete specimen. In addition, here, the surrounding metal matrix can deform more easily under the influence of the electrostatic pressure arising from the electric field. When there were more than two nanoparticles simultaneously imaged on the detector, the specimen immediately fractured. This suggests that the ratio of the exposed surface of $BaTiO_3$ nanoparticles to Ni matrix is an essential factor for successful measurement.

The atomic-scale elemental mapping of $BaTiO_3$ helps identifying impurities on the particles' surface that could be problematic in achieving reliable high-yield manufacturing. During sintering, grain boundaries form along interfaces between adjacent particles, removing pores by surface diffusion at high temperature [45]. Impurities at the particle's surface can be trapped and decorate the grain boundaries, thereby modifying their properties [46]. In recent studies on the grain boundary engineering, the residual impurities on the colloidal nanocrystals surface segregated at grain boundaries during coarsening eventually change the nanomaterial's charge transport properties [47,48]. As Na acts as a dopant in $BaTiO_3$ [28,49] tuning the material's dielectric constant, ferromagnetic, and optical properties, the surface contamination on the pre-processed particles can be another factor that affect the intrinsic property of as-sintered $BaTiO_3$, calling for great caution.

Declaration of Competing Interest

The authors declare that they have no known competing financial interests or personal relationships that could have appeared to influence the work reported in this paper.

Acknowledgments

S.-H.K. and B.G. acknowledge financial support from the DFG through DIP Project No. 450800666. X.Z. is grateful for financial support from the Alexander von Humboldt Foundation. Theoretical calculation was supported by the National Research Foundation of Korea (NRF) funded by the Ministry of Education (NRF-2021R1A6A1A03043682). The calculations were supported by the Welch Foundation (F-1841) and the Texas Advanced Computing Center.

Supplementary materials

Supplementary material associated with this article can be found, in the online version, at doi:10.1016/j.scriptamat.2023.115370.

References

[1] H. Jaffe, Titanate ceramics for electromechanical purposes, Ind. Eng. Chem. 42 (1950) 264–268, https://doi.org/10.1021/ie50482a020.
[2] W. Liu, X. Ren, Large piezoelectric effect in Pb-free ceramics, Phys. Rev. Lett. 103 (2009), 257602, https://doi.org/10.1103/PhysRevLett.103.257602.
[3] D.-.Y. Lu, X.-.L. Gao, S. Wang, Abnormal Curie-temperature shift in Ho-doped BaTiO3 ceramics with the self-compensation mode, Results Phys. 12 (2019) 585–591, https://doi.org/10.1016/j.rinp.2018.11.094.
[4] T. Kimura, Q. Dong, S. Yin, T. Hashimoto, A. Sasaki, T. Sato, Synthesis and piezoelectric properties of Li-doped BaTiO3 by a solvothermal approach, J. Eur. Ceram. Soc. 33 (2013) 1009–1015, https://doi.org/10.1016/j.jeurceramsoc.2012.11.007.
[5] M. Chen, Z. Xu, R. Chu, Z. Wang, S. Gao, G. Yu, W. Li, S. Gong, G. Li, Y2O3-modified Ba(Ti0.96Sn0.04)O3 ceramics with improved piezoelectricity and raised Curie temperature, Mater. Res. Bull. 59 (2014) 305–310, https://doi.org/10.1016/j.materresbull.2014.07.040.
[6] M. Adamczyk-Habrajska, B. Wodecka-Duś, T. Goryczka, D. Szalbot, M. Bara, Ł. Ciepły, Dielectric and electric properties of Ba0.996 La0.004 Ti0.999 O3 ceramics doped with europium and hafnium ions, Materials (Basel) 15 (2022), https://doi.org/10.3390/ma15020413.
[7] W. Cai, C.L. Fu, J.C. Gao, C.X. Zhao, Dielectric properties and microstructure of Mg doped barium titanate ceramics, Adv. Appl. Ceram. 110 (2011) 181–185, https://doi.org/10.1179/1743676110Y.0000000019.
[8] M.H. Khedhri, N. Abdelmoula, H. Khemakhem, R. Douali, F. Dubois, Structural, spectroscopic and dielectric properties of Ca-doped BaTiO3, Appl. Phys. A. 125 (2019) 193, https://doi.org/10.1007/s00339-019-2487-y.
[9] L. Huang, Z. Jia, I. Kymissis, S. O'Brien, High K capacitors and OFET gate dielectrics from self-assembled BaTiO3 and (Ba,Sr)TiO3 nanocrystals in the superparaelectric limit, Adv. Funct. Mater. 20 (2010) 554–560, https://doi.org/10.1002/adfm.200901258.
[10] F.D. Morrison, D.C. Sinclair, A.R. West, Doping mechanisms and electrical properties of La-doped BaTiO3 ceramics, Int. J. Inorg. Mater. 3 (2001) 1205–1210, https://doi.org/10.1016/S1466-6049(01)00128-3.
[11] M. Cernea, O. Monnereau, P. Llewellyn, L. Tortet, C. Galassi, Sol–gel synthesis and characterization of Ce doped-BaTiO3, J. Eur. Ceram. Soc. 26 (2006) 3241–3246, https://doi.org/10.1016/j.jeurceramsoc.2005.09.039.
[12] A. YAMAJI, Y. ENOMOTO, K. KINOSHITA, T. MURAKAMI, Preparation, characterization, and properties of Dy-doped small-grained BaTiO3 ceramics, J. Am. Ceram. Soc. 60 (1977) 97–101, https://doi.org/10.1111/j.1151-2916.1977.tb15479.x.
[13] M. Liu, H. Hao, Y. Zhen, T. Wang, D. Zhou, H. Liu, M. Cao, Z. Yao, Temperature stability of dielectric properties for xBiAlO3–(1−x)BaTiO3 ceramics, J. Eur. Ceram. Soc. 35 (2015) 2303–2311, https://doi.org/10.1016/j.jeurceramsoc.2015.02.015.
[14] P. Vuollo, J. Honkamo, M. Niemelä, P. Perämäki, H. Jantunen, Determination of boron and lithium in ferroelectric samples by ICP-OES and ICP-MS, Microchim. Acta. 164 (2009) 217–224, https://doi.org/10.1007/s00604-008-0061-y.
[15] J. Zhang, A. Visinoiu, F. Heyroth, F. Syrowatka, M. Alexe, D. Hesse, H.S. Leipner, High-resolution electron energy-loss spectroscopy of BaTiO3/SrTiO3 multilayers, Phys. Rev. B. 71 (2005) 64108, https://doi.org/10.1103/PhysRevB.71.064108.
[16] M. Bugnet, G. Radtke, S.Y. Woo, G. Zhu, G.A. Botton, High energy-resolution EELS of ferroelectric and paraelectric BaTiO3 phases, in: Eur. Microsc. Congr. 2016 Proc, 2016, pp. 935–936, https://doi.org/10.1002/9783527808465.EMC2016.6645.
[17] V. Ischenko, E. Pippel, R. Köferstein, H.-.P. Abicht, J. Woltersdorf, Barium titanate via thermal decomposition of Ba,Ti-precursor complexes: the nature of the intermediate phases, Solid State Sci 9 (2007) 21–26, https://doi.org/10.1016/j.solidstatesciences.2006.09.004.
[18] A. Kirianov, T. Hagiwara, H. Kishi, H. Ohsato, Effect of Ho/Mg ratio on formation of core-shell structure in $BaTiO_3$and on dielectric properties of $BATIO_3$CERAMICS, Jpn. J. Appl. Phys. 41 (2002) 6934–6937, https://doi.org/10.1143/jjap.41.6934.
[19] S. Fuentes, R.A. Zárate, E. Chávez, P. Muñoz, M. Ayala, R. Espinoza-González, P. Leyton, Synthesis and characterization of BaTiO3 nanoparticles in oxygen atmosphere, J. Alloys Compd. 505 (2010) 568–572, https://doi.org/10.1016/j.jallcom.2010.06.074.
[20] R.A. De Souza, C. Voisin, H. Schraknepper, M. Teusner, M. Kessel, P. Dufour, C. Tenailleau, S. Guillemet-Fritsch, Complex diffusion behavior of oxygen in nanocrystalline BaTiO3 ceramics, Phys. Chem. Chem. Phys. 16 (2014) 2568–2575, https://doi.org/10.1039/C3CP53979B.
[21] T. Bräuniger, T. Müller, A. Pampel, H.-.P. Abicht, Study of oxygen−nitrogen replacement in BaTiO3 by 14N solid-state nuclear magnetic resonance, Chem. Mater. 17 (2005) 4114–4117, https://doi.org/10.1021/cm050411k.
[22] B. Gault, A. Chiaramonti, O. Cojocaru-Mirédin, P. Stender, R. Dubosq, C. Freysoldt, S.K. Makineni, T. Li, M. Moody, J.M. Cairney, Atom probe tomography, Nat. Rev. Methods Prim. (2021) 1–51, https://doi.org/10.1038/s43586-021-00047-w.
[23] J.H. Kim, K. Jang, D.-.K. Lim, S. Ahn, D. Oh, H. Kim, J. Seo, P.-.P. Choi, W. Jung, Self-assembled nano-composite perovskites as highly efficient and robust hybrid cathodes for solid oxide fuel cells, J. Mater. Chem. A. 10 (2022) 2496–2508, https://doi.org/10.1039/D1TA08178K.
[24] J.B. Seol, C.M. Kwak, Y.T. Kim, C.G. Park, Understanding of the field evaporation of surface modified oxide materials through transmission electron microscopy and atom probe tomography, Appl. Surf. Sci. (2016), https://doi.org/10.1016/j.apsusc.2016.01.196.
[25] S. Kim, S. Antonov, X. Zhou, L. Stephenson, C. Jung, A. El-Zoka, D.K. Schreiber, S. Conroy, B. Gault, J. Mater, S.-.H. Kim, S. Antonov, X. Zhou, L.T. Stephenson, C. Jung, A.A. El-Zoka, D.K. Schreiber, M. Conroy, B. Gault, Atom probe analysis of electrode materials for Li-ion batteries: challenges and ways forward, J. Mater. Chem. A. 6 (2022) 4883–5230, https://doi.org/10.1039/D1TA10050E.
[26] J.S. Chappell, T.A. Ring, J.D. Birchall, Particle size distribution effects on sintering rates, J. Appl. Phys. 60 (1986) 383–391, https://doi.org/10.1063/1.337659.
[27] A.Thompson Thompson, D. Attwood, E. Gullikson, M. Howells, K.-.J. Kim, J. Kirz, J. Kortright, I. Lindau, Y. Liu, P. Pianetta, A. Robinson, J. Scofield, J. Underwood,

G. Williams, H. Winick, X-ray Data Booklet, Lawrence Berkeley Natl. Lab, 2009, p. 176.
[28] S.M. Yakout, Influence of Na and Na/Fe doping on the dielectric constant, ferromagnetic and sunlight photocatalytic properties of BaTiO3 perovskite, J. Solid State Chem. 290 (2020), 121517, https://doi.org/10.1016/j.jssc.2020.121517.
[29] A. Debnath, S.K. Lalwani, S. Singh, Sunny, Improvement in ferroelectric properties of BaTiO3 film by mn/sr doping for non-volatile memory applications, Micro and Nanostructures 171 (2022), 207421, https://doi.org/10.1016/j.micrna.2022.207421.
[30] S.-.H. Kim, P.W. Kang, O.O. Park, J.-.B. Seol, J.-.P. Ahn, J.Y. Lee, P.-.P. Choi, A new method for mapping the three-dimensional atomic distribution within nanoparticles by atom probe tomography (APT), Ultramicroscopy 190 (2018) 30–38, https://doi.org/10.1016/j.ultramic.2018.04.005.
[31] Samsung Electro-Mechanics, MLCC (Multilayer Ceramic Capacitors), Samsung Electro-Mechanics, 2022.
[32] K. Thompson, D. Lawrence, D.J. Larson, J.D. Olson, T.F. Kelly, B. Gorman, In situ site-specific specimen preparation for atom probe tomography, Ultramicroscopy 107 (2007) 131–139, https://doi.org/10.1016/j.ultramic.2006.06.008.
[33] W. Eiser, H.P. Beck, Trace analysis of impurities in sol-gel prepared BaTiO3-powders with ICP-MS, Fresenius. J. Anal. Chem. 364 (1999) 417–421, https://doi.org/10.1007/s002160051359.
[34] J. Heyd, G.E. Scuseria, M. Ernzerhof, Hybrid functionals based on a screened Coulomb potential, J. Chem. Phys. 118 (2003) 8207–8215, https://doi.org/10.1063/1.1564060.
[35] R. Tazaki, D. Fu, M. Itoh, M. Daimon, S. Koshihara, Lattice distortion under an electric field in $BaTiO_3$piezoelectric single crystal, J. Phys. Condens. Matter. 21 (2009), 215903, https://doi.org/10.1088/0953-8984/21/21/215903.
[36] T.A. Field, I. Microscope, elastic deformation of field-ion- microscope tips, 2070 (2007) 10–13.
[37] K.D. Rendulic, E.W. Müller, Twinning of iridium in a field ion microscope, J. Appl. Phys. 37 (1966) 2593–2595, https://doi.org/10.1063/1.1782089.
[38] C.K.S. Moy, G. Ranzi, T.C. Petersen, S.P. Ringer, Macroscopic electrical field distribution and field-induced surface stresses of needle-shaped field emitters, Ultramicroscopy 111 (2011) 397–404, https://doi.org/10.1016/j.ultramic.2011.01.024.
[39] T.J. Wilkes, J.M. Titchmarsh, G.D.W. Smith, D.A. Smith, R.F. Morris, S. Johnston, T.J. Godfrey, P. Birdseye, The fracture of field-ion microscope specimens, J. Phys. D. Appl. Phys. 5 (1972) 2226–2230, https://doi.org/10.1088/0022-3727/5/12/312.
[40] J.D. Jackson, Classical Electrodynamics, 1925-2016, 3rd ed., Wiley, New York, 1999, https://search.library.wisc.edu/catalog/999849741702121.
[41] T.J. Prosa, S. Strennen, D. Olson, D. Lawrence, D.J. Larson, A study of parameters affecting atom probe tomography specimen survivability, Microsc. Microanal. 25 (2019) 425–437, https://doi.org/10.1017/S1431927618015258.
[42] D.R. Clark, H. Zhu, D.R. Diercks, S. Ricote, R.J. Kee, A. Almansoori, B.P. Gorman, R.P. O'Hayre, Probing grain-boundary chemistry and electronic structure in proton-conducting oxides by atom probe tomography, Nano Lett. 16 (2016) 6924–6930, https://doi.org/10.1021/acs.nanolett.6b02918.
[43] S. Pedrazzini, A.J. London, B. Gault, D. Saxey, S. Speller, C.R.M. Grovenor, M. Danaie, M.P. Moody, P.D. Edmondson, P.A.J. Bagot, Nanoscale stoichiometric analysis of a high-temperature superconductor by atom probe tomography, Microsc. Microanal. 23 (2017) 1–11, https://doi.org/10.1017/S1431927616012757.
[44] C. Jung, H. Jun, K. Jang, S.-.H. Kim, P.-.P. Choi, Tracking the Mn diffusion in the carbon-supported nanoparticles through the collaborative analysis of atom probe and evaporation simulation, Microsc. Microanal. 28 (2022) 1841–1850, https://doi.org/10.1017/S1431927622012211.
[45] R.K. Bordia, S.-J.L. Kang, E.A. Olevsky, Current understanding and future research directions at the onset of the next century of sintering science and technology, J. Am. Ceram. Soc. 100 (2017) 2314–2352, https://doi.org/10.1111/jace.14919.
[46] D. Raabe, M. Herbig, S. Sandlöbes, Y. Li, D. Tytko, M. Kuzmina, D. Ponge, P. P. Choi, Grain boundary segregation engineering in metallic alloys: a pathway to the design of interfaces, Curr. Opin. Solid State Mater. Sci. 18 (2014) 253–261, https://doi.org/10.1016/j.cossms.2014.06.002.
[47] D. Cadavid, S. Ortega, S. Illera, Y. Liu, M. Ibáñez, A. Shavel, Y. Zhang, M. Li, A. M. López, G. Noriega, O.J. Durá, M.A. López De La Torre, J.D. Prades, A. Cabot, Influence of the ligand stripping on the transport properties of nanoparticle-based PbSe nanomaterials, ACS Appl. Energy Mater. (2020), https://doi.org/10.1021/acsaem.9b02137.
[48] S.-.H. Kim, S.-.H. Yoo, P. Chakraborty, J. Jeong, J. Lim, A.A. El-Zoka, X. Zhou, L. T. Stephenson, T. Hickel, J. Neugebauer, C. Scheu, M. Todorova, B. Gault, Understanding alkali contamination in colloidal nanomaterials to unlock grain boundary impurity engineering, J. Am. Chem. Soc. 144 (2022) 987–994, https://doi.org/10.1021/jacs.1c11680.
[49] M. Soni, M. Saleem, N. Bajpai, S. Chouhan, M.D. Varshney, A. Mishra, Structural and optical properties on Na doped BaTiO3, in: AIP Conf. Proc 2100, 2019, p. 20185, https://doi.org/10.1063/1.5098739.